Quaternary International 459 (2017) 165–174

Contents lists available at ScienceDirect

Quaternary International

journal homepage: www.elsevier.com/locate/quaint

Sensitivity of southern hemisphere westerly wind to boundary conditions for the last glacial maximum

Seong-Joong Kim*, Sang-Yoon Jun, Baek-Min Kim

Korea Polar Research Institute, KORDI, PO Box 32, Incheon, 406-840, South Korea

ARTICLE INFO

Article history:
Received 28 October 2016
Received in revised form
21 March 2017
Accepted 3 April 2017
Available online 20 April 2017

Keywords:
Southern hemisphere
Last glacial maximum
Westerly winds
Surface temperature
CMIP5

ABSTRACT

The southern hemisphere (SH) westerly wind change in the LGM is critical in understanding the glacial-interglacial carbon cycle since its strength and position influence the upwelling of the carbon rich deep water to the surface. To examine the change in SH westerly wind in the LGM, we adopted CAM5 atmosphere general circulation model (GCM) and performed LGM simulation with sensitivity experiments by specifying the LGM sea ice in the Southern Ocean (SO), ice sheet over Antarctica, and tropical pacific sea surface temperature. The SH westerly response to LGM boundary conditions in the CAM5 was compared with those from CMIP5 LGM simulations. In the CAM5 LGM simulation, the SH westerly wind substantially increases between 40°S and 65°S, while the zonal-mean zonal wind decreases at latitudes higher than 65°S. The position of the SH maximum westerly wind moves poleward by about 8° in the LGM simulation. Sensitivity experiments suggest that the increase in SH westerly winds is mainly due to the increase in sea ice in the SO that accounts for 60% of total wind change. In the CMIP5-PMIP3 LGM experiments, most of the models show the slight increase and poleward shift of the SH westerly wind as in the CAM5 experiment. The increased and poleward shifted westerly wind in the LGM obtained in the current model result is consistent with previous model results and some lines of proxy evidence, though opposite model responses and proxy evidence exist for the SH westerly wind change.

1. Introduction

The atmosphere carbon dioxide concentration (CO_2) has increased continuously since the industrialization and it is expected to increase in the future. The glacial-interglacial climate fluctuation is linked to cyclic changes in orbital parameters of the Earth, but the energy budget from the change in orbital parameters is not enough to account for the magnitude of the glacial-interglacial climate change. The change in atmospheric CO_2 modulated the glacial-interglacial climate change by feedback mechanism (Kim et al., 1998; Sigman and Boyle, 2000; Ahn and Brook, 2008). During the Last Glacial Maximum (LGM), occurred about 21,000 years before present (ka BP), the atmospheric CO_2 was lower than at present by about 80 ppmv. While the naturally varied atmospheric CO_2 amount (about 80 ppmv) from interglacial to glacial time is smaller than the artificially increased atmosphere CO_2 after industrialization (about 100 ppmv), the cause of the glacial reduction of atmospheric CO_2 remains controversial.

There have been numerous hypotheses to account for the magnitude of glacial CO_2 reduction including biological and chemical pumps, but toward present, hypotheses based on the Southern Ocean (SO) barrier has become more popular (Sigman and Boyle, 2000; Toggweiler et al., 2006; Toggweiler and Russell, 2008; Toggweiler, 2009; Anderson et al., 2009). The reason behind the importance of the SO in the glacial CO_2 budget is associated with the upwelling rate of carbon rich water from the deep ocean to the surface that could play as a source or sink of atmospheric CO_2 (Toggweiler et al., 2006). In the SO, air-sea CO_2 flux can be modulated by the strength of the vertical mixing, that influences the upwelling of dissolved inorganic carbon to the surface. The oceanic eddy activity also plays an important role in modulating the air-sea CO_2 flux by shallowing or thickening of the mixed layer depths (Song et al., 2016).

The strength of upwelling is determined by the position and strength of the westerly wind. During the LGM, the temperature reduction in the SO is much larger than the tropics, where temperature changed little. This stronger equator-pole temperature gradient should give a stronger zonal winds and consequent stronger ocean circulation and ventilation (old deep ocean water is replaced by newly produced water in the polar oceans). However,

* Corresponding author.
E-mail address: seongjkim@kopri.re.kr (S.-J. Kim).

http://dx.doi.org/10.1016/j.quaint.2017.04.001
1040-6182/

proxy evidence shows that during glacial time, ocean circulation was slower (Lynch-Stieglitz et al., 2007) and ventilation was weaker (Sikes et al., 2009). Liu et al. (2015) claim that the oceanic upwelling is driven by low-level wind stress rather than westerly winds and the de-correlation between the winds and wind stress could be due to the expanded sea ice towards equator in the LGM by undermining the efficacy of wind in generating wind stress. The mismatch between the ocean circulation and wind change in the LGM is not clearly resolved, but it is obvious that the understanding of wind change is crucial.

The location and strength of the southern hemisphere (SH) westerly are important in determining the SO upwelling rate, that consequently influences the glacial-interglacial carbon cycles. To investigate whether there was any change in the location and strength of SH westerly winds in the LGM, both observation and modelling efforts have been given. One school of observation evidence has suggested the northward shift of westerly winds. Toggweiler (2009) claimed that in the LGM, the westerly wind axis was displaced to equatorward. Since the Antarctic Circumpolar Current (ACC) is constrained by the Drake Passage, the northward wind shift would weaken the SO upwelling and thus leads to the reduction of dissolved inorganic carbon (DIC) concentration at the surface. This subsequently plays a role in reducing atmospheric CO_2 with less outgassing. By analyzing lacustrine palynologic records along the western Chile, McCulloch et al. (2000) suggested the northward wind shift. By analyzing pollen types using the sample from the south America, Moreno et al. (1999) also obtained the northward displaced SH westerly wind by 7–10° in the LGM. From data compilation, Kohfeld et al. (2013) suggested the 3–5° shift to the north. Heusser (1989) also obtained a northward shift of the SH westerlies. The northward shift of SH westerly winds was illustrated by the cooler tropical temperature than in the SO that weaken the Hadley cell circulation and its downward branch shifted equatorward (Toggweiler and Russell, 2008), or equatorward compression of frontal bands by the increase in sea ice cover around Antarctica in the LGM (Chiang and Bitz, 2005).

On the other hand, another school of evidence suggests opposite results, i.e. poleward shifts of SH westerly winds in the LGM (e.g., Markgraf, 1987, 1989; Harrison, 1993; Harrison and Dodson, 1993). Note, however, that the local moisture-based terrestrial records has a high uncertainty in indicating a change in SH westerly wind as shown in the contrasting results of Heusser (1989) and Markgraf (1989) and this uncertainty is from the local orographic effect on moisture distribution (Liu et al., 2015).

Numerical experiments have been performed to examine the change in the westerly winds in its strength and position and as in the data reconstructions, the model results are varying from model to model. Using Canadian Center for Climate Modelling and Analysis (CCCma) coupled Atmosphere-Ocean General Circulation Model, Kim et al. (2002, 2003) obtained the equatorward shift of the SH westerly winds. Using another AOGCM, Williams and Bryan (2006) also obtained the same response. However, using NCAR and MRI AOGCMs, Shin et al. (2003) and Kitoh et al. (2001) obtained the poleward shift of SH westerly winds, respectively. Using NCAR AGCM-only model (CCM3) with prescribed LGM boundary conditions, Kim and Lee (2009) obtained the 3–4° equatorward shift. Using AOGCM-only models, Drost et al. (2007) obtained equatorward shift, whereas Wyrwoll et al. (2000) obtained poleward shift. By analyzing the model results from the second phase of Paleoclimate Modelling Intercomparison Project (PMIP2), different SH wind responses were obtained (Rojas et al., 2009).

Besides the location of the SH westerly wind, a change in its strength is important as well in driving the Ekman pumping of the SO water. Toggweiler et al. (2006) and Toggweiler and Russell (2008) suggested weakening of the SH westerly wind in the LGM, associated with the larger cooling in the tropics relative to the polar regions that gives a decrease in meridional temperature gradient. The weakening of the wind is also consistent with the enhanced ocean stratification during the LGM (Burke and Robinson, 2012). However, another study suggested the stronger glacial winds associated with the increase in meridional pressure gradient by the large equator-to-pole temperature gradient (e.g., McGee et al., 2010). Dust records from ice core suggest a strengthened westerly during the LGM (e.g., De Angelis et al., 1987; Petit et al., 1999; Delmonte et al., 2002; Wolff et al., 2006).

Numerical model results are different as well. Using CCCma AOGCM, Kim et al. (2002, 2003) obtained a weaker westerly winds in the SH in the LGM. Using NCAR CCM3 AGCM with prescribed SST and sea ice conditions from CLIMAP (1981) reconstructions, Kim and Lee (2009) obtained the weaker SH westerly wind by 20–30%. However, there have been evidence for the stronger SH westerly wind from numerical simulation and proxy records. Using NCAR CGCMs, Shin et al. (2003) and Otto-Bliesner et al. (2006) obtained stronger SH westerly winds. Some authors claimed that the SO westerly winds were intensified in the LGM due to an increase in the equator-to-pole temperature gradient (e.g., Keeling and Visbeck, 2001).

As summarized above, the location and strength of the SH westerly wind in the LGM remains still unclear, though their information is critical in accounting for the atmosphere CO_2 budget. In this study, we examined the responses of SH westerly winds to LGM boundary conditions using the state-of-the-art numerical model. To evaluate which boundary conditions are more important in the position and strength of SH westerly winds, we also attempted sensitivity experiments by setting glacial sea ice, ice sheet, and tropical SST conditions.

2. Models and experiments

In this study, we used NCAR Community Atmosphere Model version 5 (CAM5), which is the latest version in a series of global atmosphere models developed at National Center for Atmospheric Research (NCAR) for numerical experiments. CAM5 improves significantly the representation of atmospheric processes with model physics of CAM version 4. As the atmosphere subcomponent of CESM1.0, CAM5 includes more realistic formulations of radiation, boundary layer, and aerosols compared to CAM version 4 (CAM4). The aerosol scheme is prognostic (Liu et al., 2012) and cloud microphysics includes both direct and indirect effect of sulfate and black and organic carbon (Morrison and Gettelman, 2008; Gettelman et al., 2010). We utilize CAM5 with model physics of CAM4 in order to maintain consistency with CCSM4 experiment from the CMIP5, which used CAM4 physics and provides surface boundary conditions of sea surface temperature and sea-ice cover to this study. This configuration using consistent physical processes will help to reduce an uncertainty in simulation due to air-sea decoupling compared to the CCSM4 experiment in the CMIP5. There is time–evolving land use change in the twentieth and twenty-first century climate simulations (Lawrence et al., 2011). Finite volume dynamical core with $1.9° \times 2.5°$ horizontal resolution and 26 hybrid sigma vertical level is adopted in this study.

Table 1 lists experimental setup that included in the current study. The preindustrial simulation (PI) includes orbital parameters and land surface boundary conditions for the preindustrial time that are provided by CMIP5 experimental design. Sea surface temperature (SST) and sea ice conditions are from CCSM4 experiment, which was used in the CMIP5 experiment. The last glacial maximum experiment referred to as LGM includes orbital parameters for 21,000 years ago and LGM SST and sea ice conditions obtained from CCSM4 experiment for the CMIP5 experiment. We also

Table 1
Brief summary of experimental design.

Experiment name	Orbital parameters and greenhouse gases condition	Land surface condition	SST/sea-ice condition
PI	PI[a]	PI[a]	PI[a]
LGM	LGM[b]	LGM[b]	Climatology taken from CCSM4 LGM experiment for the CMIP5
S_SEAICE	PI[a]	PI[a]	PI[a] except for climatological sea-ice concentration over southern hemisphere taken from CCSM4 LGM experiment for the CMIP5
A_ICESHEET	PI[a]	PI[a] except for ice-sheet condition over the Antarctic region from LGM[b]	PI[a]
EQ_SST	PI[a]	PI[a]	PI[a] except for climatological SST over pacific equatorial region (from 20 S to 20 N) taken from CCSM4 LGM experiment for the CMIP5

[a] Conditions from pi-control scenario provided by CMIP5 experimental design.
[b] Conditions from for LGM scenario provided by CMIP5-PMIP3 experimental design.

examined the sensitivity of the SH westerly to the change in sea ice concentration for the LGM over the SO from the CCSM4 and this experiment is called S_SEAICE. The sensitivity experiment to the change in LGM ice sheet conditions over Antarctica, that was provided from PMIP3 experimental setup, is referred to as A_ICEHSHEET. Finally, we investigated the sensitivity of the SH westerly winds to the change in tropical SST for the LGM taken from CCSM4 LGM experiment and this experiment is called EQ_SST.

Fig. 1 displays the change in boundary conditions in austral winter (June-July-August) between the LGM, S_SEAICE, A_ICESHEET, EQ_SST and PI experiments, respectively. Since the largest response to changes in LGM boundary conditions occurs in austral winter, the June-July-August averaged results will only be presented in this study. In Fig. 1a, contour lines display the change in SST whose largest reduction occurs in the SO next to the expanded sea ice. The sea ice change over the SO and ice sheet changes in Antarctica and Andes mountains are represented as crosses and shadings, respectively. The biggest sea ice expansion and ice sheet increase occurs in the Bellingshausen and Amundsen Seas. Note that in the LGM experiment, both Laurentide ice sheet and Arctic sea ice expansion shown in Fig. S1 is included because northern hemisphere boundary conditions are also important in modulating the SH westerly wind and atmospheric CO_2 as suggested by a model study (Lee et al., 2011). Other figures in Fig. 1 represents the forcings for sensitivity experiments of sea ice change for the SO, Antarctic ice sheet change, and SST change in the tropics. In these sensitivity experiments, we excluded northern hemisphere boundary conditions to isolate the effect of the change in boundary condition for the southern hemisphere. Thus the LGM total change is not necessarily the same quantity of the sum of results from sensitivity experiments.

All experiments were integrated for 30 years, and the entire period of results was analyzed. Initial conditions for the LGM simulation were created by spin-up integration for 250 years, and initial conditions for PI were provided from CESM repository as spun-up state. In the sensitivity experiments, these initial conditions were used with boundary conditions.

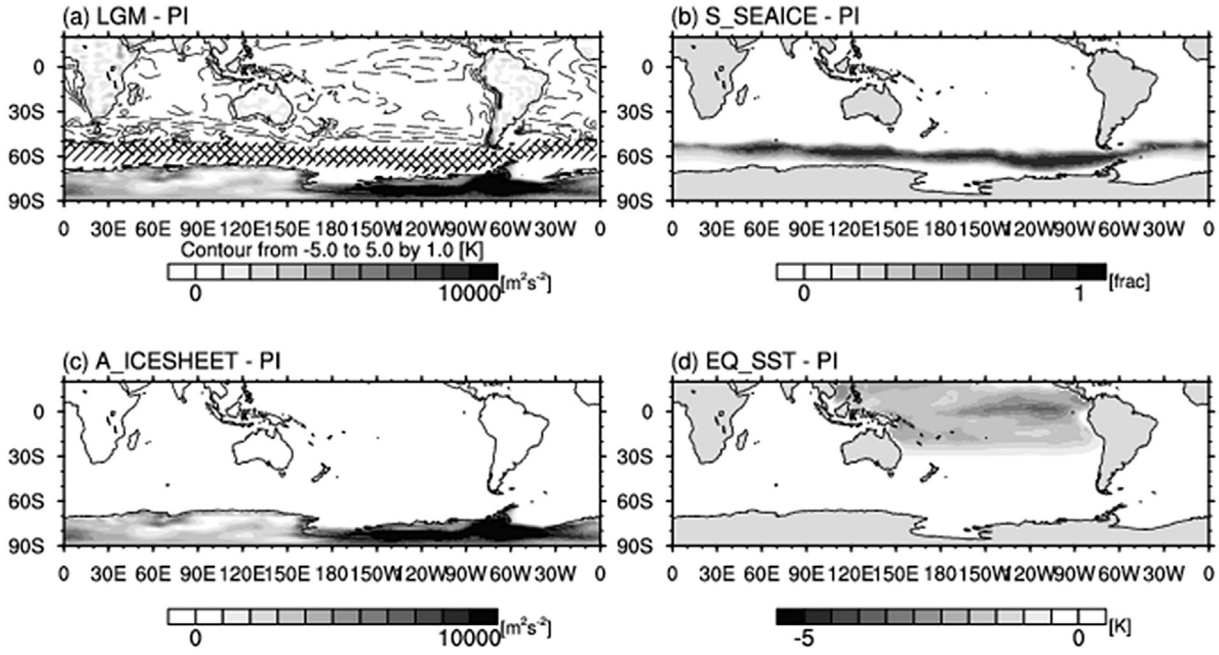

Fig. 1. Austral winter (June-July-August) forcing from LGM, S_SEAICE, A_ICESHEET, and EQ_SST experiments compared to PI experiment. (a) surface geopotential (shading), sea surface temperature (contour), and sea-ice concentration (oblique and cross-checked; above 0.1 and above 0.5, respectively), (b) sea-ice concentration, (c) surface geopotential, and (d) sea surface temperature.

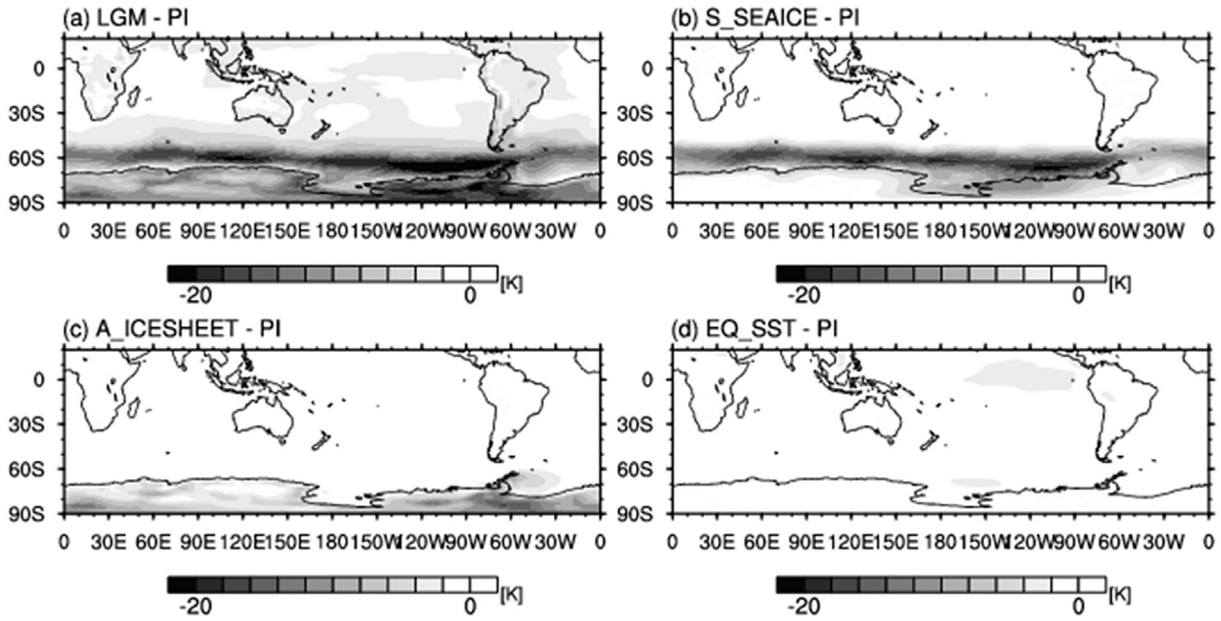

Fig. 2. Changes in austral winter (June-July-August) mean surface air temperature from (a) LGM, (b) S_SEAICE, (c) A_ICESHEET, and (d) EQ_SST experiments compared to the PI experiment.

3. Results

Fig. 2 presents changes in austral winter (averaged for June-July-August) surface air temperature (SAT) between LGM, S_SEAICE, A_ICESHEET, EQ_SST, and PI experiments. In the LGM winter, SAT decreases substantially as would be expected. The biggest reduction of SAT reaches −20 °C such as the Amundsen Sea and Bellingshausen Sea and west Antarctica in winter (Fig. 2a). The annual-mean LGM surface temperature reduction ranges from −4 °C to −16 °C (Fig. S2). Regions for the substantial temperature reduction such as west Antarctica occurs in places where the sea ice and ice sheet increase substantially (Fig. 1b and c). There have been efforts in reconstructing the surface temperature change using ice core analyses in the LGM for Antarctica (Petit et al., 1999; Stenni et al., 2001; Kawamura et al., 2007). These studies obtained SAT change between −8 °C and −10 °C. The simulated annual-mean SAT reduction is slightly overestimated in comparison to the observed proxy records, but it is overall consistent with other model results (e.g., IPCC, 2013).

Fig. 3 displays changes in temperature and zonal-mean zonal wind in the vertical section from troposphere to stratosphere. In the LGM, the large reduction in temperature occurs in lower troposphere, which shows dome-shape reduction profile with biggest reduction between 50°S and 70°S at the surface associated with the increase in sea ice and at around 700 hPa level at latitudes higher than 75°S associated with the increase in ice sheet. At lower stratosphere, temperature reduction is about 5 °C, while in lower latitudes temperature increases slightly by about 2 °C. In PMIP2 model experiments, most model shows an increase in temperature at lower stratosphere in higher latitudes that is different from the current experiment, but in lower latitudes temperature increases by about 2 °C as in the present result (Kim et al., 2014).

In the LGM, the zonal mean zonal wind appears to increase between 40°S and 70°S from troposphere to stratosphere, while it is reduced at latitudes lower than 40°S and higher than 70°S (Fig. 3a). The biggest strengthening occurs at about 60°S at upper troposphere level (250 hPa) where in the LGM zonal-mean zonal wind increases by more than 10 ms^{-1}. Sensitivity experiments show that the biggest contribution to the increase in SH zonal-mean zonal winds in the LGM is by the increase in sea ice, which explains about 60% of the total change (Fig. 3b). The increase in Antarctic ice sheet contributes to the increase in zonal winds at stratosphere level, but it contributes to the slight decrease in winds at high southern latitudes at lower troposphere (Fig. 3c). The SST reduction in the tropics increases the zonal mean zonal wind at stratosphere levels at around 60°S, while it weakens the wind at southern latitudes higher than 70°S (Fig. 3d). In the LGM, the zonal mean zonal wind increases in the upper troposphere levels around the equator and this is mainly due to the reduced SST in the tropics. In summary, the strengthening of the zonal mean zonal wind in the LGM is mainly due to the increase in sea ice and secondarily due to the reduced SST in the tropics.

In order to compare CAM5 results with the CMIP5-PMIP3 LGM experiments, we prepared the change in temperature and the zonal mean zonal wind for austral winter between the LGM and PI experiments from 7 CMIP5-PMIP3 models of CCSM4, CNRM-CM5, FGOALS-g2, IPSL-CM5A-LR, MIROC-ESM, MPI-ESM-P, MRI-CGCM3 (Fig. 4). In the CMIP5 LGM experiments, the cooling of dome-shaped profile over Antarctica and the SO is consistently found in all models as also shown in our experiment, but degree of cooling in CMIP5-PMIP3 models is smaller in stratosphere in low latitudes than in our case or opposite to the change simulated in our experiment in high southern latitudes (Fig. 3a). As in our experiment, however, the zonal-mean zonal wind increases between 40°S and 70°S in all CMIP5-PMIP3 models, but its strengthening is much less than our experiment and even less than the results of CCSM for PMIP2 experiment where maximum reduction of the zonal mean zonal wind is more than 5 ms^{-1} (Kim et al., 2014). These differences seem to be due to different model versions and boundary conditions.

To examine the change in SH westerly winds in more detail, we examined the zonal-mean zonal winds at upper troposphere (200 hPa) and lower troposphere (850 hPa). At upper level, the zonal-mean zonal wind increase substantially at around 60°S by more than 10 ms^{-1}, especially off west Antarctica (Fig. 5a), mainly due to the increase in sea ice (Fig. 5b). The reduced SST also

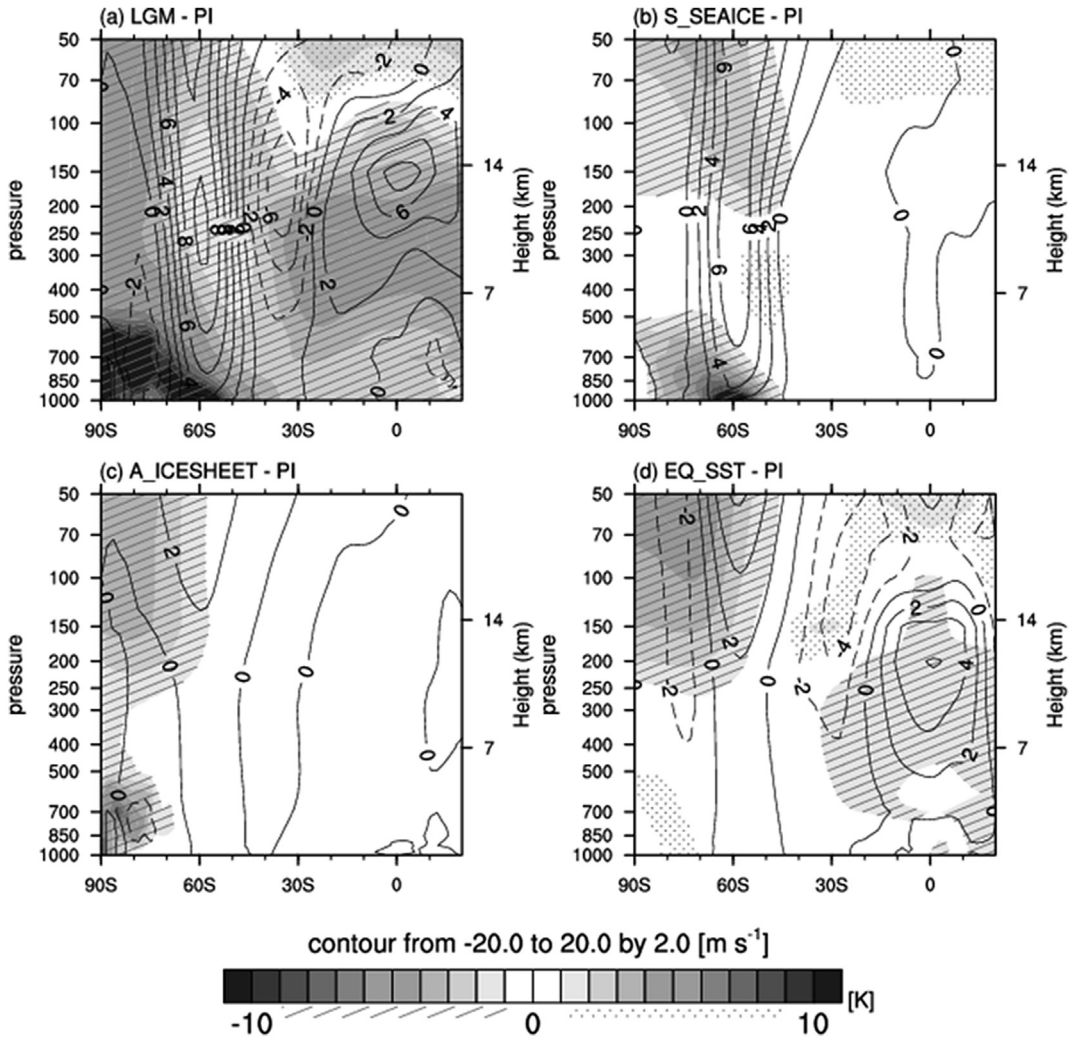

Fig. 3. Changes in zonally averaged temperature (shading) and zonal wind (contour) from (a) LGM, (b) S_SEAICE, (c) A_ICESHEET, and (d) EQ_SST experiments compared to the PI experiment.

contributed to the increase in the zonal-mean zonal wind at the Pacific sector of the Southern Ocean between 60°W and 180° (Fig. 5d), where the increase in zonal-mean zonal winds is part of Rossby wave train initiated from the tropical Pacific. The reduced SST in the tropical Pacific leads to the increase in the zonal-mean zonal wind in low latitudes and gives the decrease at 30°S and increase and decrease again toward the high southern latitudes. It is widely known that the west Antarctic temperature response is sensitive to a change in tropical Pacific temperature (e.g., Ding et al., 2011).

CMIP5-PMIP3 LGM experiments all show the slight increase in the upper level zonal-mean zonal wind at 60°S (Fig. 6), with the biggest increase in the MRI-CGCM3 by about 6 ms^{-1} (Fig. 6g). The change in the zonal-mean zonal wind in CMIP5 is much smaller than in our experiment where zonal-mean zonal wind at 60°S decreases by more than 10 ms^{-1} (see Fig. 5a). Another notable difference is that unlike our experiment, upper-level warming is simulated by most of CMIP5-PMIP3 models. In spatial pattern, the MRI-CGCM3 shows the most similar result with our experiment. Liu et al. (2015) and Rojas (2013) found that the CCSM4 and MRI-CGCM3 simulate the distributions of SH westerly and Antarctic sea ice with greater fidelity than other CMIP5-PMIP3 models. Even though the degree of change in zonal-mean zonal win in CMIP5-PMIP3 LGM experiments is different from our model result, all models show the increase in winds at latitudes higher than 50°S and the decrease at about 30°S-50°S.

The change in zonal-mean zonal winds at lower level (850 hPa) shows the substantial increase at about 60°S (Fig. 7a), associated with the increased sea ice in the SO (Fig. 7b) and in part by the reduced tropical SST, which mostly influences the wind change at the Pacific sector associated with the Rossby wave teleconnection (Fig. 7d). The change in Antarctic ice sheet shows some modification of the zonal winds over Antarctica, but it is relatively small. Fig. 8 presents that most CMIP5-PMIP3 model results show the slight increase in the zonal-mean zonal wind in the Southern Ocean except for the MIROC and MPI models where a slight weakening is found as also found in previous studies (Chavaillaz et al., 2013; Liu et al., 2016).

In addition to the strength of the SH westerly wind, the position change to the LGM forcing is important in determining the upwelling rate in the SO deep water. To identify the position of the SH westerly in the PI and LGM sensitivity experiments, and in the CMIP5-PMIP3 LGM experiments, we prepared the latitudinal variation of zonal-mean winds for the LGM, PI, and sensitivity experiments using CAM5 and LGM experiment in CAM5 is compared with those from CMIP5-PMIP3 models (Fig. 9). In the CAM5 experiment,

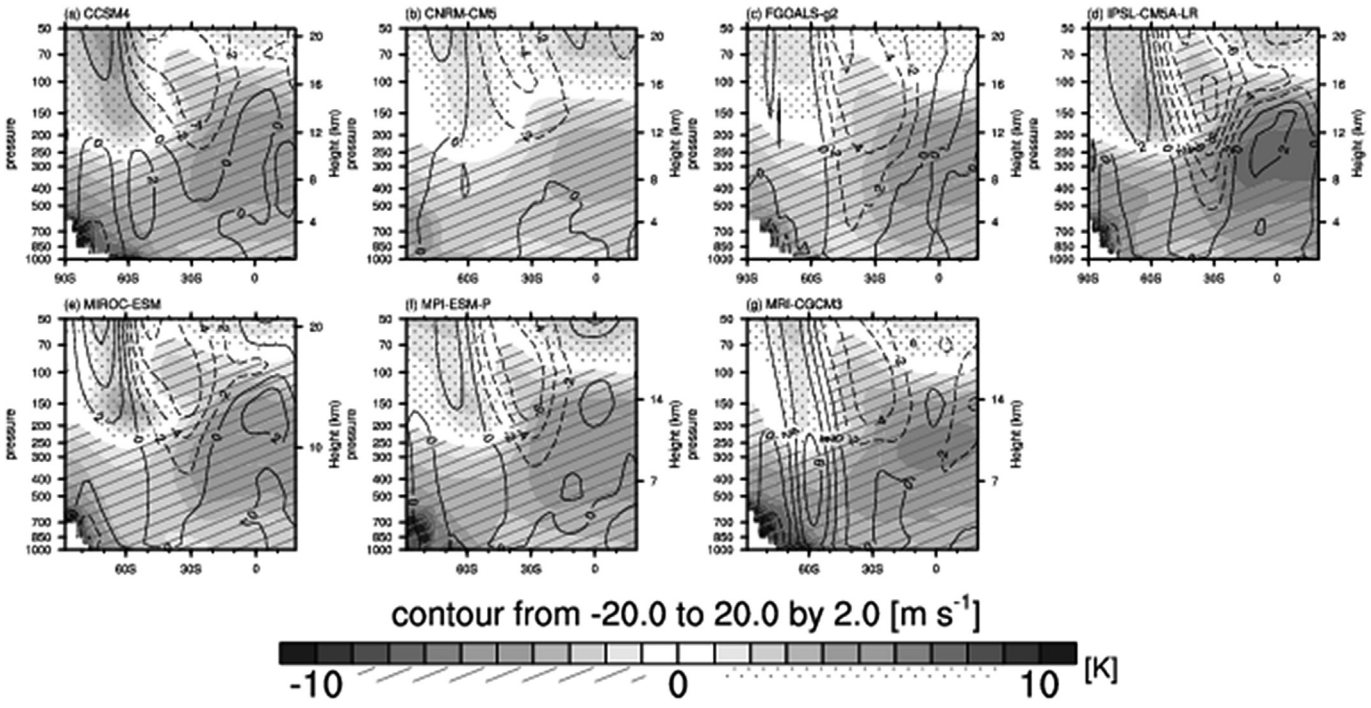

Fig. 4. Changes in zonally averaged temperature (shading) and zonal wind (contour) from LGM experiment compared to PI experiment by 7 CMIP5 models: (a) CCSM4, (b) CNRM-CM5, (c) FGOALS-g2, (d) IPSL-CM5A-LR, (e) MIROC-ESM, (f) MPI-ESM-P, and (g) MRI-CGCM3.

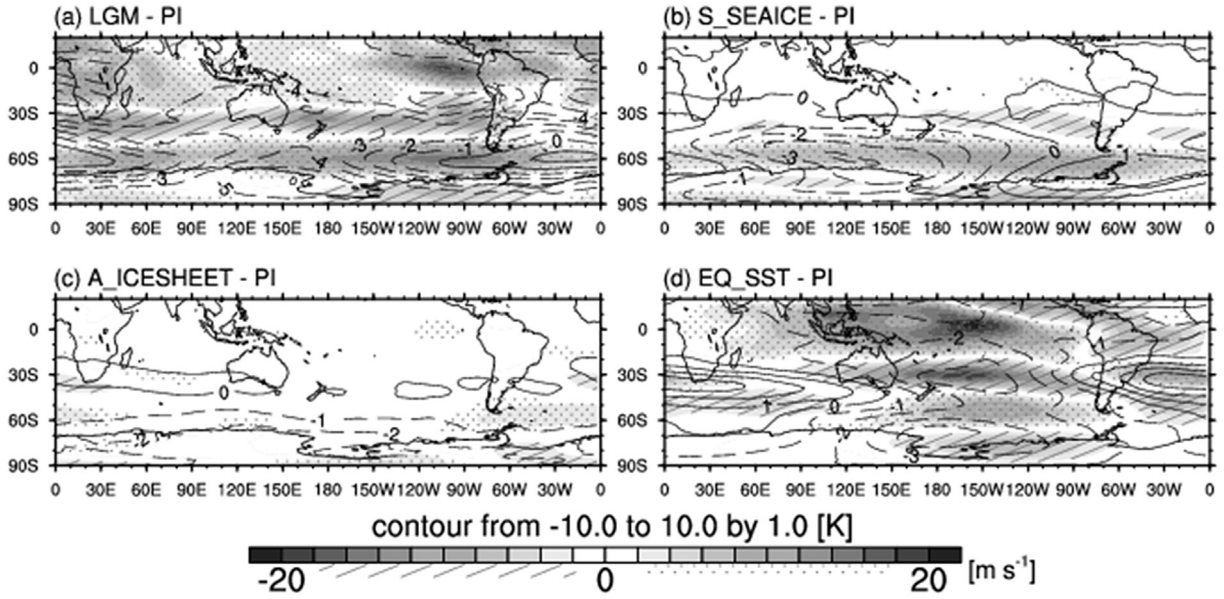

Fig. 5. Changes in temperature (contour) and zonal wind (shading) at 200 hPa from (a) LGM, (b) S_SEAICE, (c) A_ICESHEET, and (d) EQ_SST experiments compared to the PI experiment.

the maximum westerly wind is located at around 45°S in the PI case, while it is displaced to the south to around 53°S in the LGM experiment with about 8° poleward movement. As in the change in the westerly wind strength, the change in sea ice in the LGM account for the largest portion of the poleward displacement of the maximum wind position (Fig. 9a). Other forcings do not contribute to the movement of the SH westerly winds. In the coupled model simulation for the LGM from CMIP5-PMIP3 experiments, all models show either slight poleward displacement or almost no change in the position. Again the MRI-CGCM3 model is most similar to our experiment with about 5° shift to the south in the LGM. Overall, model results analyzed in this study show that in the LGM the SH westerly wind increases and is displaced to the south.

4. Discussion

This study investigates the change in SH westerly winds at the LGM that is critical in determining the strength of the SO upwelling of carbon rich water from the deep ocean to the surface. Some recent studies have suggested that the SH westerly winds were

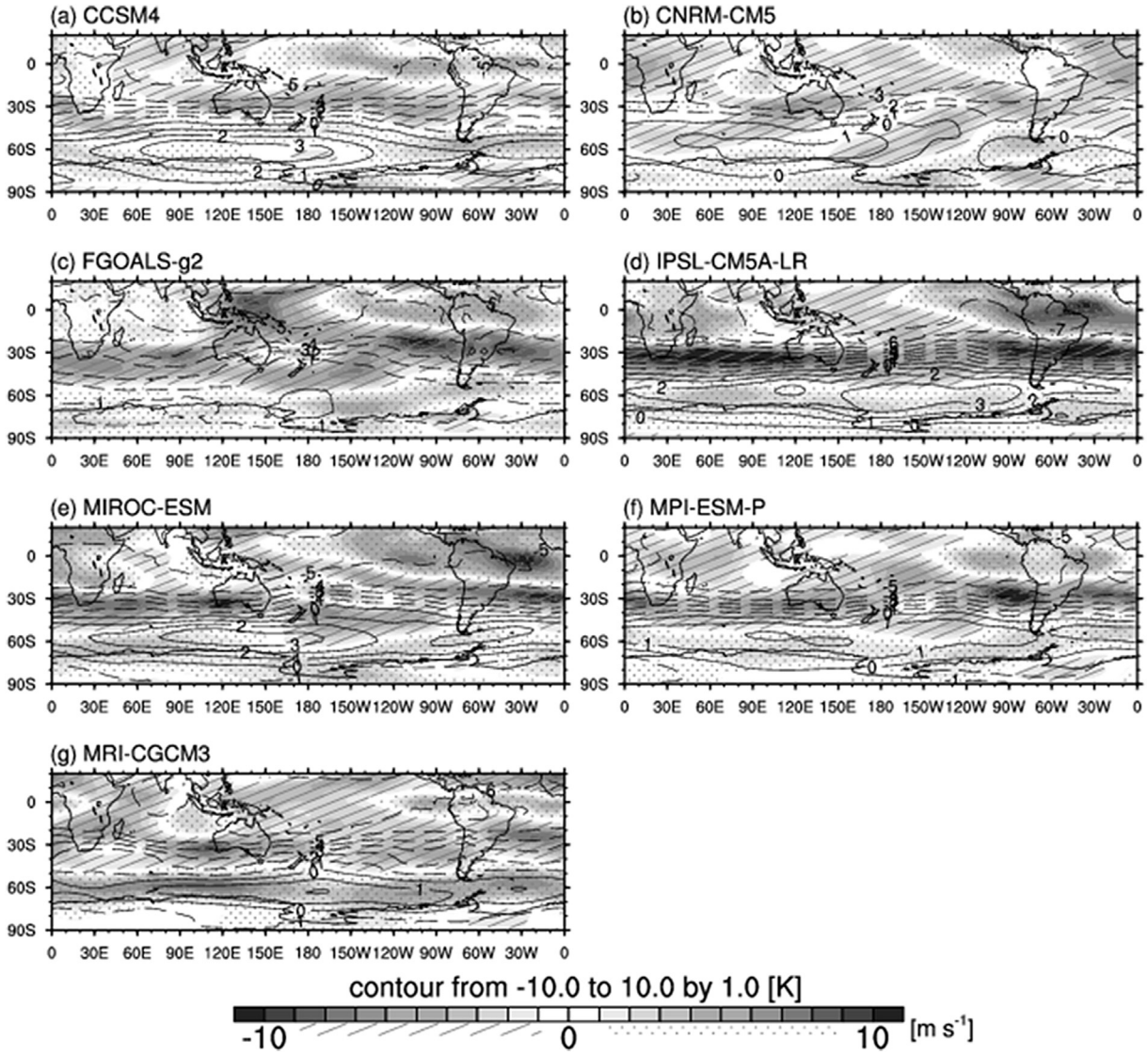

Fig. 6. Changes in temperature (contour) and zonal wind (shading) at 200 hPa from LGM experiment compared to PI experiment by 7 CMIP5 models: (a) CCSM4, (b) CNRM-CM5, (c) FGOALS-g2, (d) IPSL-CM5A-LR, (e) MIROC-ESM, (f) MPI-ESM-P, and (g) MRI-CGCM3.

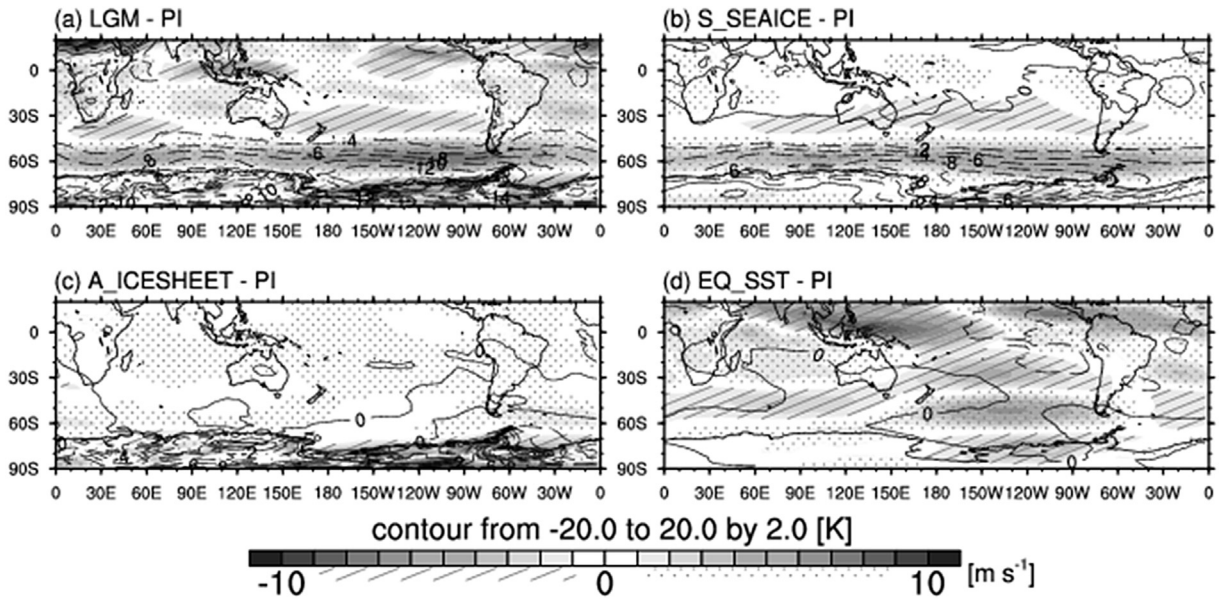

Fig. 7. Changes in temperature (contour) and zonal wind (shading) at 850 hPa from (a) LGM, (b) S_SEAICE, (c) A_ICESHEET, and (d) EQ_SST experiments compared to the PI experiment.

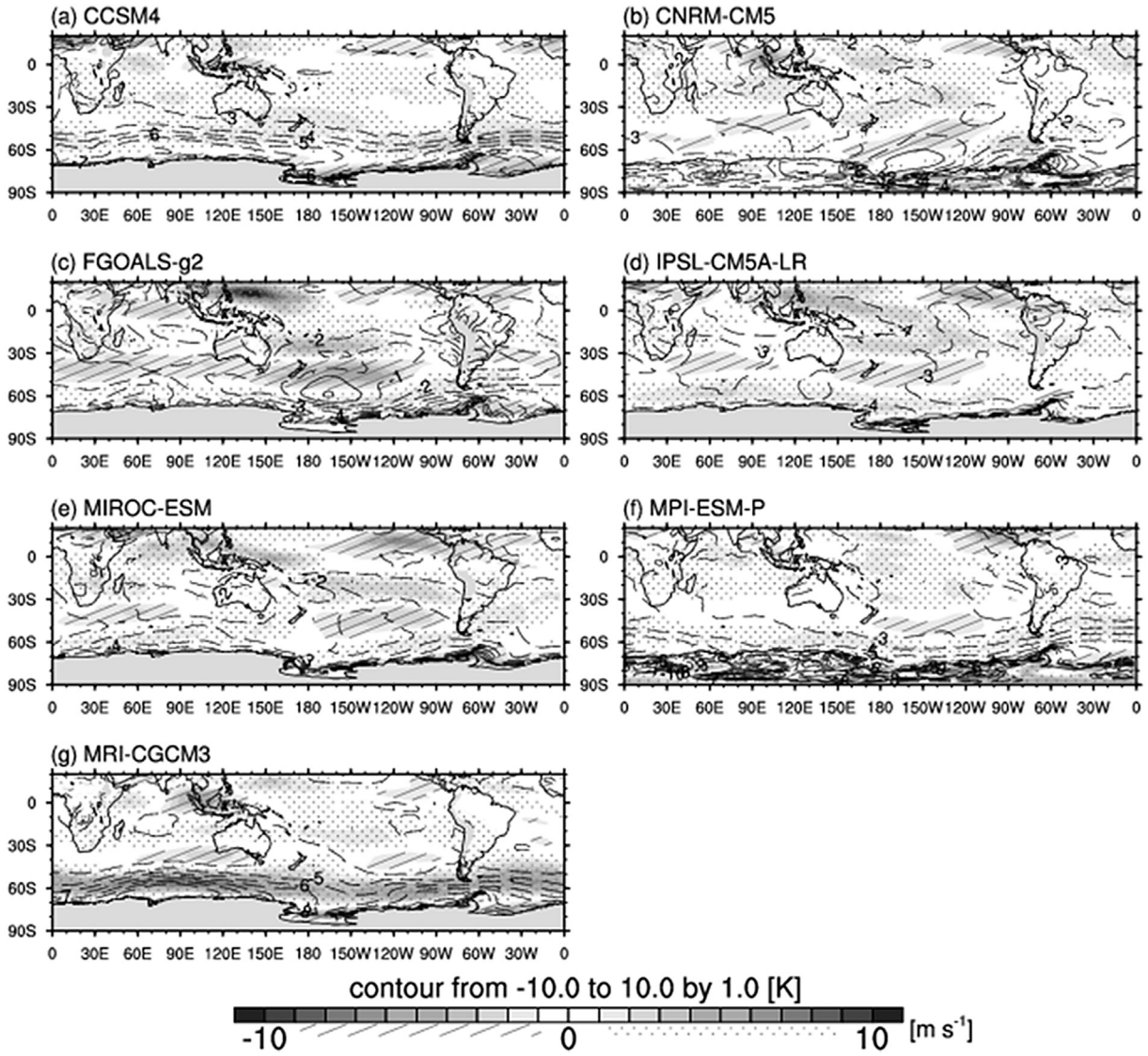

Fig. 8. Changes in temperature (contour) and zonal wind (shading) at 850 hPa from LGM experiment compared to PI experiment by 7 CMIP5 models: (a) CCSM4, (b) CNRM-CM5, (c) FGOALS-g2, (d) IPSL-CM5A-LR, (e) MIROC-ESM, (f) MPI-ESM-P, and (g) MRI-CGCM3.

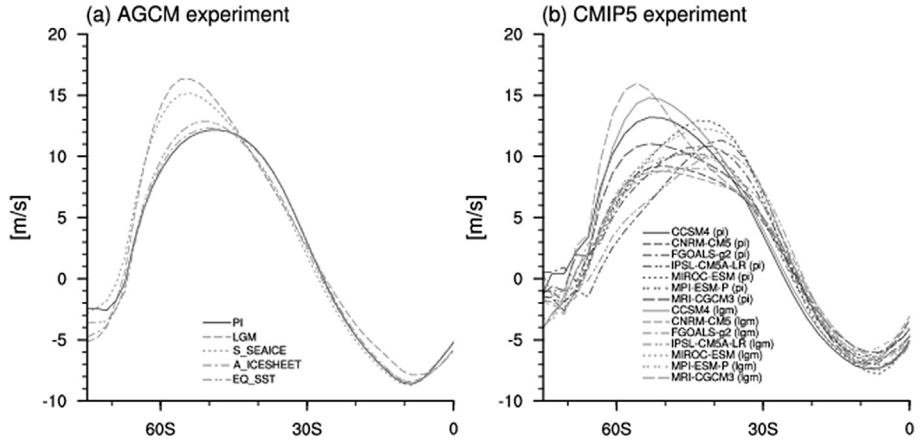

Fig. 9. Zonally averaged zonal wind at 850 hPa from (a) PI, LGM, S_SEAICE, A_ICESHEET, and EQ_SST experiments, and (b) PI and LGM experiments by 7 CMIP5 models. Dark-gray lines in both panels indicate PI experiments and light-gray lines indicate LGM and forced experiments in left panel, and LGM experiments in right panel.

weaker than present and displaced to the equator by 5–10° that weakens upwelling of the SO, acting as a barrier (Toggweiler and Russell, 2008; Toggweiler, 2009). However, these hypotheses have been hampered by the varying proxy evidence and model results (Kohfeld et al., 2013). We revisited to examine the SH westerly winds with LGM boundary conditions by adopting the state-of-the-art atmosphere general circulation model developed from NCAR and performed a series of control and sensitivity experiments. The results obtained in this study is not quite different from other atmosphere GCM experiments, not included in this study. For example, using Hadley center atmosphere GCM, Sime et al. (2013) simulated SH westerly wind changes during the LGM and obtained increases of SH westerly winds poleward of 50°S. This result is virtually the same results as our experiment even though their change in the wind magnitude is smaller than our case. As described above, all atmosphere-ocean coupled models included in the CMIP5-PMIP3 LGM simulations show the increase in westerly winds even though there are some various amplitudes in the difference.

Another indirect hint for the LGM SH westerly wind strength and position could be obtained from its change under ongoing and future global warming, because the climate response to the greenhouse gas increase mirrors that of the colder climate background like LGM (Kim et al., 2003). The change in westerly winds since the industrialization is suggested to become stronger than before industrialization. For example, using the Geophysical Fluid Dynamics Laboratory (GFDL) coupled general circulation model, Kushner et al. (2001) obtained an intensified westerly winds from surface to 250 hPa over the southern hemisphere in future 21st century. Yin (2005) and Fyfe and Saenko (2006) analyzed climate models reported in the IPCC and obtained a remarkably consistent strengthening and poleward shifting of the zonal wind axis through the 20th and 21st centuries. Russell et al. (2006) also obtained poleward intensification of SH westerly winds under the greenhouse gas increase. Using high-resolution ocean GCM, Biastoch et al. (2009) obtained the increase in Aguhlas leakage due to poleward shift of SH westerlies. These results suggest that the hypothesis by Toggweiler (2009) is reasonable.

Then we need to ponder whether there is anything missing in the AGCM or AOGCM model simulations. Using CCCma AOGCM, Kim et al. (2002, 2003) obtained the weaker and equatorward shift of westerly winds. Using NCAR CCM3 AGCM with prescribed SST and sea ice conditions for the LGM from the CLIMAP (1979) reconstruction, Kim and Lee (2009) obtained the weaker westerly winds and slight shift toward the equator. Even though there is some difference in physics in the model between CCM3 and CAM5, the bigger difference seems to be the SST and sea ice change. Kim and Lee (2009) concluded that the sea ice increase in the LGM leads to a substantial cooling around Antarctica, that weakens equator-pole temperature gradient and consequently westerly winds. However, this argument is still weak because Figs. 7 and 8 shows that the CAM5 AGCM model results and some CMIP5-PMIP3 coupled model results, such as CCSM4, MPI-ESM-P, and MRI-CGCM3, show the substantial cooling around Antarctica in the LGM as in Kim and Lee (2009), but they all obtained the increase in the SH westerly winds.

The discrepancy between the hypothesis by Toggweiler (2009) of weaker and equatorward shift of SH westerly winds in the LGM and model results with some proxy evidence remains to be uncertain and need to be explored further in future study. The key outcome in our experiments is that the change in sea ice, which includes the effect of atmospheric CO_2 reduction, plays the most important role in determining the change in the LGM SH westerly winds, and secondarily the change in tropical Pacific SST in determining the change in westerly wind in the Pacific sector of the Southern Ocean.

5. Summary and conclusion

We investigate the change in SH westerly winds in the LGM using the state-of-the-art CAM5 AGCM from NCAR with prescribed LGM boundary conditions from CCSM4 CMIP5-PMIP3 experiment. We performed sensitivity experiments with specified sea ice conditions over the SO, Antarctic ice sheet, and tropical Pacific SST conditions from 20°S to 20°N for the LGM.

In response to the prescribed boundary conditions for the LGM, the SH westerly wind increases substantially in the SO from troposphere to stratosphere, while the zonal-mean zonal wind decreases over Antarctica and subtropical regions. The increase in SH westerly winds is mainly due to the increase in sea ice in the SO that accounts for the 60% of total wind change. Similar results were obtained by the CMIP5-PMIP3 LGM experiments using atmosphere-ocean coupled GCMs, i.e. all models show the increase in SH westerly winds in the LGM, but the degree of wind increase is smaller than the current experiment except for the MRI GCM, which shows the most similar result to our current experiment.

In terms of the position of the SH westerly wind in the LGM, our model experiments show that the maximum wind is displaced to the south by about 8°, mainly due to the increase in sea ice over the SO in the LGM. In the CMIP5-PMIP3 LGM experiments, most of the models show also the poleward shift of the SH westerly wind, especially the MRI which shows the most similar response to the CAM5 experiment.

In conclusion, in the LGM the SH westerly winds simulated to be stronger than PI, but this results is different from the hypothesis suggested by earlier studies. Reasons for this discrepancy are not clear and need to be further studied. Sensitivity experiments suggest that the change in sea ice over the SO mainly accounts for the total wind change in the LGM.

Acknowledgements

This study was supported by projects of Investigation for the cause of regional climate differences in Antarctica (PE17010) of KOPRI.

Appendix A. Supplementary data

Supplementary data related to this article can be found at http://dx.doi.org/10.1016/j.quaint.2017.04.001.

References

Ahn, J., Brook, E.J., 2008. Atmospheric CO2 and climate on millennial time scales during the last glacial period. Science 322, 83–85.
Anderson, R.F., Ali, S., Bradtmiller, L.I., Nielsen, S.H., Fleisher, M.Q., Anderson, B.E., Burckle, L.H., 2009. Wind-driven upwelling in the Southern Ocean and the deglacial rise in atmospheric CO_2. Science 323 (5920), 1443–1448.
Biastoch, A., Boning, C.W., Schwarzkopf, F.U., Lutjeharms, J.R.E., 2009. Increase in Agulhas leakage due to poleward shift of Southern Hemisphere westerlies. Nature 462, 495–498.
Burke, A., Robinson, L.F., 2012. The Southern Ocean's role in carbon exchange during the last deglaciation. Science 335, 557–561.
Chavaillaz, Y., Codron, F., Kageyama, M., 2013. Southern westerlies in LGM and future (RCP4.5) climates. Clim. Past 9, 517–524.
Chiang, J.C.H., Bitz, C.M., 2005. Influence of high latitude ice cover on the marine Intertropical Convergence Zone. Clim. Dyn. 25, 477–496.
CLIMAP, 1981. Seasonal Reconstructions of the Earth's Surface at the Last Glacial Maximum. In: The Geological Society of America Map Chart Series. MC-36.
De Angelis, M., Barkov, N.I., Petrov, V.N., 1987. Aerosol concentrations over the last climatic cycle (160 kyr) from an Antarctic ice core. Nature 325, 318–321.
Delmonte, B., Petit, J.R., Maggi, V., 2002. Glacial to Holocene implications of the new 27000-year dust record from the EPICA Dome C (East Antarctic) ice core. Clim. Dyn. 18, 647–660.
Ding, Q., Steig, E., Battisti, D.S., Kuttel, M., 2011. Winter warming in West Antarctica

caused by central tropical Pacific warming. Nat. Geosci. 4, 398–403.
Drost, F., Renwick, J.A., Bhaskarane, B., Oliver, H., McGregor, J., 2007. Features of the zonal mean circulation in the southern hemisphere during the Last Glacial Maximum. J. Geophys. Res. 112, D2. http://dx.doi.org/10.1029/2005JD006811.
Fyfe, J.C., Saenko, O.A., 2006. Simulated changes in the extratropical Southern Hemisphere winds and currents. Geophys. Res. Lett. 33, L06701. http://dx.doi.org/10.1029/2005GL025332.
Gettelman, A., Liu, X., Ghan, S.J., Morrison, H., Park, S., Conley, A.J., Klein, S.A., Boyle, J., Mitchell, D.L., Li, J.-L., 2010. Global simulations of ice nucleation and ice supersaturation with an improved cloud scheme in the Community Atmosphere Model. J. Geophys. Res. 115, D18216. http://dx.doi.org/10.1029/2009JD013797.
Harrison, S.P., 1993. Late Quaternary lake-level changes and climates of Australia. Quat. Sci. Rev. 12, 211–231.
Harrison, S.P., Dodson, J., 1993. Climates of Australia and new Guinea since 18,000 yr B.P. In: Wright Jr., H.E., et al. (Eds.), Global Climates since Last Glacial Maximum. University of Minnesota Press, Minneapolis, 365–293.
Heusser, C.J., 1989. Southern westerlies during the last glacial maximum. Quat. Res. 31, 423–425.
IPCC, Climate Change, 2013. The physical science basis. In: Stocker, T.F., Qin, D., Platter, G.-K., Tignor, M., Allen, S.K., Boschung, J., Nauels, A., Xia, Y., Bex, V., Midgley, P.M. (Eds.), Contribution of Working Group I to the Fifth Assessment Report of the Intergovernmental Panel on Climate Change. Cambridge University Press, UK and NY, USA.
Kawamura, K., Parrenin, F., Lisiecki, L.E., Uemura, R., Vimeux, F., Severinghaus, J.P., Hutterli, M.A., Nakazawa, T., Aoki, S., Jouzel, J., Raymo, M.E., Matsumoto, K., Nakata, H., Motoyama, H., Fujita, S., Goto-Azuma, K., Fujii, Y., Watanabe, O., 2007. Northern hemisphere forcing of climatic cycles in Antarctica over the past 360,000 years. Nature 448, 912–916.
Keeling, R.F., Visbeck, M., 2001. Antarctic stratification and glacial CO_2. Nature 412, 605–606.
Kim, S.-J., Crowley, T.J., Stoessel, A., 1998. Local orbital forcing of Antarctic climate change during the Last Interglacial. Science 280, 728–730.
Kim, S.-J., Flato, G.M., Boer, G.J., McFarlane, N., 2002. A coupled climate model simulation of the Last Glacial Maximum, Part 1: Transient multi-decadal response. Clim. Dyn. 19, 515–537.
Kim, S.-J., Flato, G.M., Boer, G.J., 2003. A coupled climate model simulation of the Last Glacial Maximum, Part 2: approach to equilibrium. Clim. Dyn. 20, 635–661.
Kim, S.-J., Lee, B.Y., 2009. Westerly winds in the Southern Ocean during the Last glacial maximum simulated in CCM3. Ocean Polar Res. 31 (4), 297–304.
Kim, S.-J., Lu, J.-M., Kim, B.-M., 2014. The Southern Annular Mode (SAM) in PMIP2 simulations for the last glacial maximum. Adv. Atmos. Sci. 31, 863–878.
Kitoh, A., Murakami, S., Koide, H., 2001. A simulation of the Last Glacial Maximum with a coupled atmosphere-ocean GCM. Geophys. Res. Lett. 28, 2221–2224.
Kohfeld, K.E., Graham, R.M., de Boer, A.M., Sime, L.C., Wolff, E.W., le Quere, C., Bopp, L., 2013. Southern Hemisphere westerly wind changes during the Last Glacial Maximum: paleo-data synthesis. Quat. Sci. Rev. 68, 76–95.
Kushner, P.J., Held, I., Delworth, T.L., 2001. Southern Hemisphere atmospheric circulation response to global warming. J. Clim. 14, 2238–2249.
Lawrence, D.M., Oleson, K.W., Flanner, M.G., Thornton, P.E., Swenson, S.C., Lawrence, P.J., Zeng, X., Yang, Z.-L., Levis, S., Sakaguchi, K., Bonan, G.B., Slater, A.G., 2011. Parameterization improvements and functional and structural advances in version 4 of the Community Land Model. J. Adv. Model. Earth Syst. 3, M03001. http://dx.doi.org/10.1029/2011MS000045.
Lee, S.-Y., Chiang, J.C.H., Matsumoto, K., Tokos, K., 2011. Southern wind response to North Atlantic cooling and the rise in atmospheric CO2: modeling perspective and paleoceanographic implications. Paleoceanography 26, PA1214.
Liu, W., Lu, J., Leung, R., Xie, S.-P., Liu, Z., Zhu, J., 2015. The de-correlation of westerly winds and westerly-wind stress over the Southern Ocean during the Last Glacial Maximum. Clim. Dyn. 45, 3157–3168.
Liu, X., Easter, R.C., Ghan, S.J., Zaveri, R., Rasch, P.J., Shi, X., Lamarque, J.-F., Gettleman, A., Morrison, H., Vitt, F., Conley, A., Park, S., Neale, R., Hanny, C., Ekman, A.M., Hess, P., Mahowald, N., Collins, W., Iacono, M.J., Bretherton, C.S., Flanner, M.G., Mitchell, D., 2012. Toward a minimal representation of aerosols in climate models: description and evaluation in the Community Atmosphere Model CAM5. Geosci. Model Dev. 5, 709–739.
Lynch-Stieglitz, J., Adkins, J.F., Curry, W.B., Dokken, T., Hall, I.R., Herguera, J.C., Hirschi, J.J.-M., Ivanova, E.V., Kissel, C., Marchal, O., Marchitto, T.M., McCave, I.N., McManus, J.F., Mulitza, S., Ninnemann, U., Peeters, F., Yu, E.-F., Zhan, R., 2007. Atlantic meridional overturning circulation during the Last Glacial Maximum. Science 316, 66–69.
Markgraf, V., 1987. Paleoenvironmental changes at the northern limit of the subantarctic Nothofagus forest, Lat 37°S, Argentina. Quat. Res. 28, 119–129.
Markgraf, V., 1989. Southern westerlies during the last glacial maximum-reply. Quat. Res. 31, 426–432.
McCulloch, R.D., Bently, M.J., Purves, R.S., Hulton, N.R.J., Sugden, D.E., Clapperton, C.M., 2000. Climatic inferences from glacial and palaeoecological evidence at the last glacial termination, southern South America. J. Quat. Sci. 15, 409–417.
McGee, D., Broecker, W.S., Winkler, G., 2010. Gustiness: the driver of glacial dustiness? Quat. Sci. Rev. 29, 2340–2350.
Morrison, H., Gettelman, A., 2008. A new two-moment bulk stratiform cloud microphysics scheme in the community atmosphere model, version 3 (CAM3). Part I: description and numerical tests. J. Clim. 21, 3642–3659. http://dx.doi.org/10.1175/2008jcli2105.1.
Moreno, P.I., Lowell, T.V., Jacobson Jr., G.L., Denton, G.H., 1999. Abrupt vegetation and climate changes during the last glacial maximum and last termination in the Chilean Lake District: a case study from Canal de la Puntilla (41°S). Geogr. Annu. Ser. 81, 285–311.
Otto-Bliesner, B.L., Brady, E., Clauzet, G., Tomas, R., Levis, S., Kothavala, Z., 2006. Last glacial maximum and Holocene climate in CCSM. J. Clim. 19, 2526–2544.
Petit, J.R., Jouzel, J., Raynaud, D., Barkov, N.I., Barnola, J.-M., Basile, I., Bender, M., Chappellaz, J., Davis, M., Delaygue, G., Delmotte, M., Kotlyakov, V.M., Legrand, M., Lipenkov, V.Y., Lorius, C., PÉpin, L., Ritz, C., Saltzman, E., Stievenard, M., 1999. Climate and atmospheric history of the past 420,000 years from the Vostok ice core, Antarctica. Nature 399, 429–436.
Rojas, M., Moreno, P., Kageyama, M., Crucifix, M., Hewitt, C., Abe-Ouchi, A., Ohgaito, R., Brady, E.C., Hope, P., 2009. The Southern westerlies during the last glacial maximum in PMIP2 simulations. Clim. Dyn. 32 (4) http://dx.doi.org/10.1007/s00382-008-0421-7.
Rojas, M., 2013. Sensitivity of Southern Hemisphere circulation to LGM and 4xCO_2 climates. Geophys. Res. Lett. 40, 1–6.
Russell, J.L., Dixon, K.W., Gnanadeskin, A., Stouffer, R.J., Toggweiler, J.R., 2006. The Southern Hemisphere westerlies in a warming world: propping open the door to the deep ocean. J. Clim. 19, 6382–6389.
Shin, S.-I., Liu, Z., Btto-Bliesner, O., Brady, E., Kutzbach, J., Harrison, S., 2003. A simulation of the Last Glacial Maximum climate change using the NCAR-CCSM. Clim. Dyn. 20, 127–151.
Sigman, D.M., Boyle, E.A., 2000. Glacial/interglacial variations in atmospheric carbon dioxide. Nature 407, 859–869.
Sikes, E.L., Howard, W.R., Samson, C.R., Mahan, T.S., Robertson, L.G., Volkman, J.K., 2009. Southern Ocean seasonal temperature and Subtropical Front movement on the South Tasman Rise in the late Quaternary. Paleoceanography 24, PA2201. http://dx.doi.org/10.1029/2008PA001659.
Sime, L.C., Kohfeld, K.E., Le Quere, C., Wolff, E.W., de Boer, A.M., Graham, R.M., Bopp, L., 2013. Southern Hemisphere westerly wind changes during the Last Glacial Maximum: model-data comparison. Quat. Sci. Rev. 64, 104–120.
Song, H., Marshall, J., Munro, D.R., Dutkiewicz, S., Sweeney, C., McGillicuddy Jr., D.J., Hausmann, U., 2016. Mesoscale modulation of air-sea CO2 flux in Drake Passage. J. Geophys. Res. http://dx.doi.org/10.1002/2016JC011714.
Stenni, B., Masson-Delmotte, V., Johnsen, S., Jouzel, J., Longinelli, A., Monnin, E., Röthlisberger, R., Selmo, E., 2001. An oceanic cold reversal during the last deglaciation. Science 293, 2074–2077.
Toggweiler, J.R., 2009. Shifting westerlies. Science 323, 1434–1435.
Toggweiler, J.R., Russell, J.L., 2008. Ocean circulation in a warming climate. Nature 45, 286–288. http://dx.doi.org/10.1038/nature06590.
Toggweiler, J.R., Russell, J.L., Carson, S.R., 2006. Midlatitude westerlies, atmospheric CO_2, and climate change during the ice ages. Paleoceanography 21, PA2005. http://dx.doi.org/10.1029/2005PA001154.
Williams, G.P., Bryan, K., 2006. Ice age winds: an aquaplanet model. J. Clim. 19, 1706–1715.
Wolff, E.W., et al., 2006. Southern Ocean sea-ice extent, productivity and iron flux over the past eight glacial cycles. Nature 440, 491–496.
Wyrwoll, K.H., Dong, B.W., Valdes, P., 2000. On the position of southern hemisphere westerlies at the Last Glacial Maximum: an outline of AGCM simulation results and evaluation of their implications. Quat. Sci. Rev. 19, 881–898.
Yin, J.H., 2005. A consistent poleward shift of the storm tracks in simulations of 21st century climate. Geophys. Res. Lett. 32, L18701. http://dx.doi.org/10.1029/2005GL023684.